This is the accepted manuscript made available via CHORUS. The article has been published as:

Plasmoid Formation in Current Sheet with Finite Normal Magnetic Component

P. Zhu and J. Raeder

Phys. Rev. Lett. **110**, 235005 — Published 7 June 2013

DOI: 10.1103/PhysRevLett.110.235005

Plasmoid Formation in Current Sheet with Finite Normal Magnetic Component

P. Zhu[1] and J. Raeder[2]
[1]*Department of Engineering Physics, University of Wisconsin-Madison, Madison, WI 53706, USA*
[2]*Department of Physics, University of New Hampshire, Durham, NH 03824, USA*

Current sheet configurations in natural and laboratory plasmas are often accompanied with finite normal magnetic component that is known to stabilize the two-dimensional resistive tearing instability in high Lundquist number regime. Recent MHD simulations indicate that the nonlinear development of ballooning instability is able to induce the formation of X-lines and plasmoids in a generalized Harris sheet with finite normal magnetic component in the high Lundquist number regime where the linear two-dimensional resistive tearing mode is stable.

Plasmoid often refers to a finite two-dimensional (2D) region of closed magnetic flux bounded by a separatrix with a single X-point [1, 2]. An isolated magnetic island in the downstream region of a Sweet-Parker current sheet is also generally called a plasmoid (e.g. [2]). Plasmoids are often found in natural and laboratory plasmas in association with various eruptive processes, such as those observed in solar corona, magnetosphere, and magnetic fusion experiments. Plasmoid formation has been believed to be the origin of substorm onset [3], and recently it has received renewed interests due to its potential roles in the universal process of fast reconnection [4]. Characteristically, a plasmoid could spontaneously form in the current sheet region with a finite magnetic field component B_n normal to the neutral sheet plane. However, it has not always been clear how a plasmoid would spontaneously form without external driver in such a current sheet configuration where no X-line pre-exists.

The formation of plasmoids has been mostly investigated for the Earth's magnetotail configuration in the context of substorm onset problem [1–3, 5–8]. In those studies the weakly 2D current sheet with finite B_n is used to model the initial static equilibrium of near-Earth magnetotail plasma. The 2D configuration becomes unstable to two-dimensional tearing-like perturbations when the plasma resistivity is sufficiently large. In its nonlinear stage, the unstable 2D resistive mode alone, which has been referred to by many as "2D tearing instability" (e.g. [9–17]) and recently as "axial tail instability" [18, 19] in the context of magnetotail plasma, can induce the formation of X-line and plasmoid. In reality, however, magnetotail current sheets are often in regimes where the effective plasma resistivity is too weak for the onset of 2D resistive tearing instability due to the strong stabilization from B_n (e.g. [15]). It has remained an interesting question how plasmoids would spontaneously form in the weakly resistive current sheets where no X-line pre-exists and the finite B_n is sufficient to stabilize 2D resistive modes.

Our recent three dimensional (3D) MHD simulations of plasmoid formation process in the current sheet with finite B_n and weak resistivity have shown significant difference from 2D simulations due to the 3D effects. In particular, the inclusion of the spatial variation in the equilibrium current direction (which is y direction in the Cartesian coordinates defined later) allows the presence of ballooning instability (e.g. [20–22]), which has demonstrated its critical roles in the plasmoid formation process in the higher Lundquist number regimes where the linear 2D resistive modes of the current sheet are stable. In those regimes the thin current sheet with finite B_n is susceptible to finite-k_y ballooning instability whose growth time scale is sub-Alfvénic. Here k_y is the wavenumber in the y direction. The nonlinear ballooning growth tends to stretch the current sheet and reduce B_n. As a consequence, magnetic X-points appear and plasmoids start to form. All k_y components, including the $k_y = 0$ component, contribute to the nonlinear ballooning growth that leads to the formation of plasmoids. These simulation results suggest a new mechanism for plasmoid formation in the current sheet with finite B_n in the high Lundquist number regimes. We briefly report and discuss these findings in this Letter.

We consider a generalized Harris sheet configuration in Cartesian coordinates (x, y, z) where $\mathbf{B}_0(x,z) = \mathbf{e}_y \times \nabla\Psi(x,z)$, $\Psi(x,z) = -\lambda \ln \dfrac{\cosh\left[F(x)\dfrac{z}{\lambda}\right]}{F(x)}$, and $\ln F(x) = -\int B_{0z}(x,0)dx/\lambda$. Here λ is the current sheet width, $\mathbf{e}_y$ the unit vector in y direction, and all other symbols are conventional. The profile of $B_n = B_{0z}(x,0)$ has a minimum region along x axis (Fig. 1). Such a configuration was previously used to model the near-Earth magnetotail [19, 23]. Unlike the conventional Harris sheet where B_n and the magnetic curvature are zero everywhere, the generalized Harris sheet equilibrium shown in Fig. 1 has regions of unfavorable magnetic curvature mostly around $z = 0$ due to the presence of finite B_n. Hence the generalized Harris sheet is susceptible to ballooning instability. Global simulations have identified signatures of both ballooning instability and axial tail instability near the minimum B_n region along x axis [18, 24], and recent MHD analysis indicates that such a configuration is indeed unstable to the axial tail instability but only in the low Lundquist number regime ($S \lesssim 10^3$) [19].

To further investigate the stability of the configuration

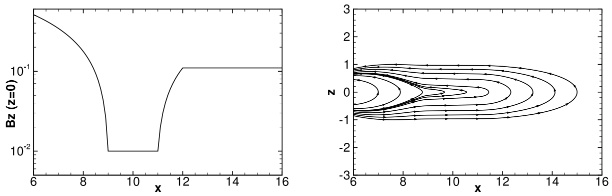

FIG. 1: $B_{0z}(x, 0)$ profile (left) and magnetic field lines (right) for the generalized Harris sheet equilibrium considered in this Letter.

in higher Lundquist number regime, a full set of resistive MHD equations are solved in 3D domain as an initial-boundary value problem

$$\frac{\partial \rho}{\partial t} + \nabla \cdot (\rho \mathbf{u}) = 0 \tag{1}$$

$$\rho \left(\frac{\partial \mathbf{u}}{\partial t} + \mathbf{u} \cdot \nabla \mathbf{u} \right) = \mathbf{J} \times \mathbf{B} - \nabla p + \mu \nabla \cdot (\rho \mathbf{w}) \tag{2}$$

$$\frac{\partial p}{\partial t} + \mathbf{u} \cdot \nabla p = -\gamma p \nabla \cdot \mathbf{u} \tag{3}$$

$$\frac{\partial \mathbf{B}}{\partial t} = -\nabla \times \mathbf{E} \tag{4}$$

$$\mathbf{E} = -\mathbf{u} \times \mathbf{B} + \eta \mathbf{J} \tag{5}$$

$$\mu_0 \mathbf{J} = \nabla \times \mathbf{B} \tag{6}$$

where ρ is the mass density, $\mathbf{u}$ the plasma flow velocity, p the pressure, $\mathbf{E}$ is the electric field, $\mathbf{B}$ is the magnetic field, $\mathbf{J}$ the current density, $J = |\mathbf{J}|$, the adiabatic index $\gamma = 5/3$, and $\mathbf{w} = \nabla \mathbf{u} + (\nabla \mathbf{u})^{\mathrm{T}} - \frac{2}{3}\mathbf{I}\nabla \cdot \mathbf{u}$. In a weakly collisional or collisionless plasma both resistivity η and viscosity μ are small in absence of anomalous sources. The above set of equations have been implemented in both the linearized and the fully nonlinear version in the NIMROD code [25] used in our computation. A solid, no-slip wall boundary condition has been imposed on the sides of the computation domain in both x and z directions, so that any potential influence from an external inward flow can be excluded. The boundary condition in the y direction is periodic. The spatial and temporal variables are normalized with the equilibrium scale length (e.g. Earth radius) and the Alfvénic time τ_{A}, respectively.

Linear calculation indicates that the current sheet configuration shown in Fig. 1 is unstable to the 2D resistive tearing or axial tail instability ($k_y = 0$) in the lower Lundquist number regime ($S \lesssim 10^3$). The inclusion of spatial variation in the y direction significantly enhances the linear growth, particularly in the higher S regime when the zero-k_y 2D resistive tearing or axial tail mode is stable (Fig. 2). The enhanced linear growth of the finite-k_y instability remains effective and becomes more relevant in the more realistic collisionality regime ($S \gtrsim 10^6$), thus making the instability a viable mechanism for explaining the faster sub-Alfvénic time scale of the current sheet evolution in situations where the sources for large anomalous resistivity are not available.

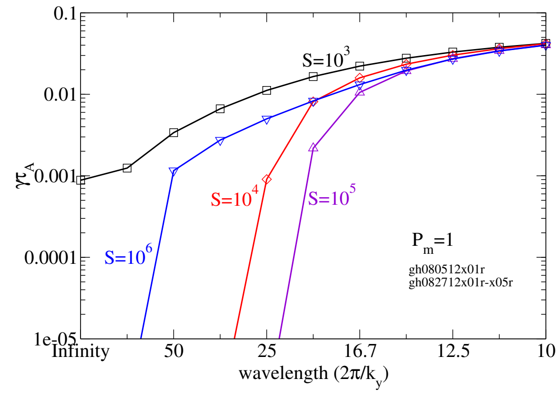

FIG. 2: Linear growth rate as function of the wavelength in y direction for different Lundquist number (S) regimes. The magnetic Prandtl number $P_m \equiv \mu/\eta = 1$ for all cases.

We now consider the nonlinear plasmoid formation process in the same current sheet configuration in a less resistive regime $S = 10^4$ where the 2D resistive tearing mode is linearly stable and a plasmoid cannot spontaneously form internally from a purely 2D process ($k_y = 0$). However, the inclusion of the 3D effects leads to an entirely new scenario where the plasmoid formation can be nonlinearly driven by a finite-k_y ballooning instability. To demonstrate such a scenario, we report results from a representative numerical case where the simulation is initialized with small magnetic perturbation whose magnitude is about one tenth of the minimum B_n. The initial perturbation is monochromatic in the y direction with a wavelength of 10. A finite element mesh of 64×64 with a polynomial degree of 5 in each direction is used for the $x - z$ domain. In the y direction, 32 Fourier collocation points are used to resolve Fourier components in the range of $0 \leq k_y L_y / 2\pi \leq 10$, where $L_y = 100$ is the domain size in y. The perturbation quickly settles into a linearly growing ballooning instability first, and subsequently drives the growth of the $k_y = 0$ component through nonlinear coupling (Fig. 3). The entire nonlinear evolution is dominated by the high k_y ($k_y L_y / 2\pi = 10$) component. A natural consequence of the nonlinear ballooning drive is the formation of plasmoids within the $x - z$ plane.

To illustrate the plasmoid formation process, we track the evolutions of the pressure contour in the $z = 0$ plane and the magnetic field lines crossing a set of fixed points along an x axis ($y = -90, z = 0$) (Fig. 4). The first stage of nonlinear evolution, as represented by the plot at $t = 180$ (the upper left panel in Fig. 4), is dominated by the growing ballooning finger-like structures in the $z = 0$ plane extending in the x direction. The magnetic field lines are mostly frozen-in to the plasma and they move along with the extending fingers, which results in a stretching and thinning of the current sheet. The re-

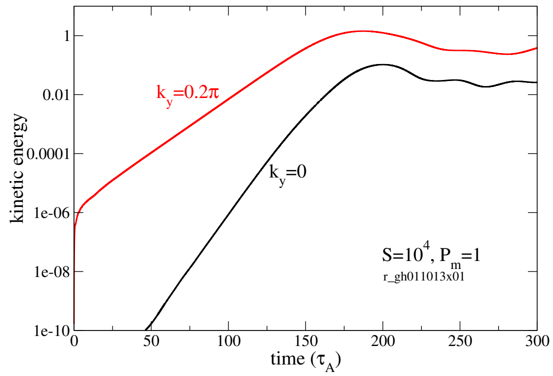

FIG. 3: Kinetic energy growth of the $k_y = 0$ (black line) and $k_y = 0.2\pi$ (red line) components of the nonlinear perturbation.

duction of the normal component B_n in the $z = 0$ plane appears to be the most in extent near the moving fronts of the extending fingers, as evidenced by the formation of a plasmoid in one of those locations around $x = 13.5$ at $t = 190$ (the upper right panel in Fig. 4). The plasmoid continues to grow in size and move in the positive x direction, even when the finger length in pressure contour has started to decrease as the amplitude of the ballooning instability has reached saturation since the time $t \simeq 190$.

In addition to the formation of plasmoid in close association with the extruding fronts of nonlinear ballooning fingers, other plasmoids have also formed in the wakes of those ballooning finger fronts (Fig. 4). Almost in parallel to the course of the plasmoid formation described in the previous paragraph, a second plasmoid starts to form since the beginning of the nonlinear ballooning saturation phase around $t = 190$ and becomes visible by $t = 200$ to $t = 210$ on those magnetic field lines crossing the $z = 0$ plane in the region around $x \simeq 9.5$ (the two middle row panels in Fig. 4). This second plasmoid however appears to be rather transient. When $t = 220$ the plasmoid located near $x \simeq 9.5$ disappears along with a dipolarization of magnetic field in that region (the lower left panel in Fig. 4). From that time, the field lines crossing the $z = 0$ plane in the $x \simeq 11$ region have started to stretch in the positive x direction, which eventually leads to the formation of a third plasmoid in that region by the time $t = 260$ (the lower right panel in Fig. 4).

Unlike in 2D simulations, the above 3D plasmoid formation process is different for different locations along y direction. For example, for a different set of field lines crossing the x axis at $y = -95, z = 0$, there is no plasmoid structure at $t = 260$ (the right panel in Fig. 5). Similarly at an earlier time $t = 200$, the plasmoid associated with the ballooning finger front at $x = 14$ on the $y = -90, z = 0$ axis (as shown in the middle left panel in Fig. 4) does not exist on these field lines crossing the $y = -95, z = 0$ axis; only near $x = 9.5$ a plasmoid structure remains with a slightly different shape (the left panel in Fig. 5). The variation of the plasmoid presence and appearance in the y direction strongly indicates that the plasmoid formation reported here is an intrinsically 3D process that is qualitatively different from the 2D process.

In summary, we demonstrated in simulations that nonlinear ballooning instability can effectively enable the formation of plasmoids in a current sheet with finite normal component in the higher Lundquist number regime where the 2D resistive tearing or axial tail mode is stabilized by the finite B_n. Our results are not limited to the specific current sheet model shown in Fig. 1 or the particular numerical settings. The scenario obtained here persists in our simulations based on the more realistic current sheet profiles that are continuous at any differential order, and in simulations with higher resolutions as well as non-monochromatic initial perturbations. We plan to report those additional simulation results elsewhere. Recent 2D and 3D kinetic simulations have also found that plasmoids can form in magnetotail configurations and regimes where the 2D resistive tearing mode itself would be stable [26–28]. The quantification of the full range of configuration and parameter space for the reported plasmoid formation mechanism, and the comparison between the MHD and kinetic simulation results will be subjects of future studies.

This research was supported by NSF grants AGS-0902360 and PHY-0821899. Work at UNH was also supported by NASA grant NAS5-02099 (THEMIS). P. Zhu is grateful for discussions with A. Bhattacharjee, J. Birn, N. Bessho, C. C. Hegna, Y.-M. Huang, C.-S. Ng, A. Otto, A. Runov, M. Sitnov, C. R. Sovinec. The computational work used the NSF XSEDE resources provided by TACC under grant number TG-ATM070010, and the resources of NERSC, which is supported by DOE under Contract No. DE-AC02-05CH11231.

[1] A. Otto, K. Schindler, and J. Birn, *J. Geophys. Res.* **95**, 15023 (1990).
[2] D. Biskamp, *Nonlinear Magnetohydrodynamics* (Cambridge University Press, Cambridge, UK, 1993).
[3] J. Birn and E. W. Hones, Jr., *J. Geophys. Res.* **86**, 6802 (1981).
[4] A. Bhattacharjee, Y.-M. Huang, H. Yang, et al., *Phys. Plasmas* **16**, 112102 (2009).
[5] L. C. Lee, Z. F. Fu, and S.-I. Akasofu, *J. Geophys. Res.* **90**, 10896 (1985).
[6] R. Hautz and M. Scholer, *Geophys. Res. Lett.* **14**, 969 (1987).
[7] M. Ugai, *Phys. Fluids B* **1**, 942 (1989).
[8] A. Kageyama, K. Watanabe, and T. Sato, Tech. Rep. NIFS-049, National Institute for Fusion Science (1990).
[9] K. Schindler, *J. Geophys. Res.* **79**, 2803 (1974).
[10] A. A. Galeev and L. M. Zelenyi, *Sov. Phys. JETP* **43**, 1113 (1976).

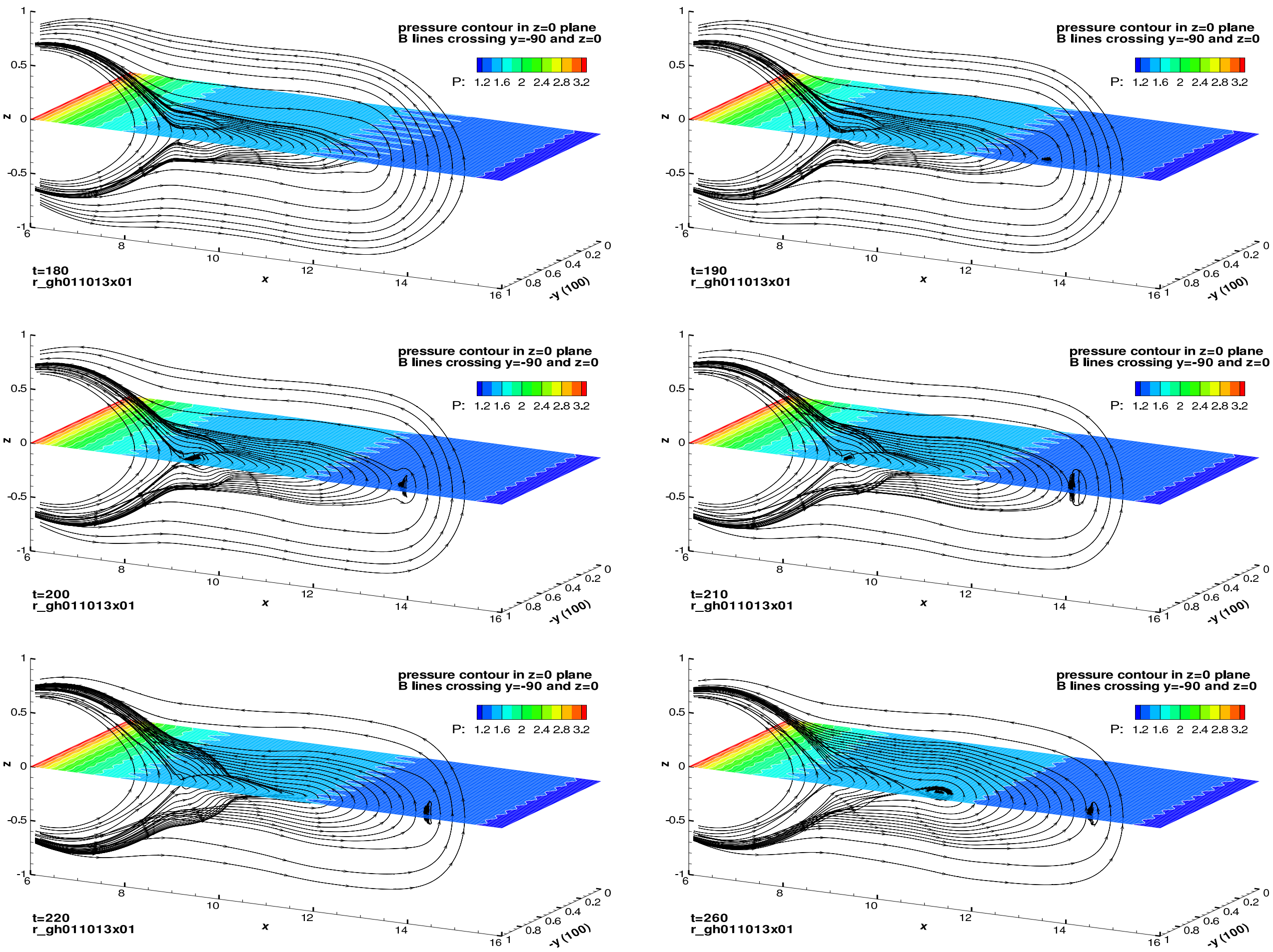

FIG. 4: Total pressure contours in the $z = 0$ plane and magnetic field lines crossing the x axis at $y = -90, z = 0$ at selected times ($t = 180, 190, 200, 210, 220, 260$).

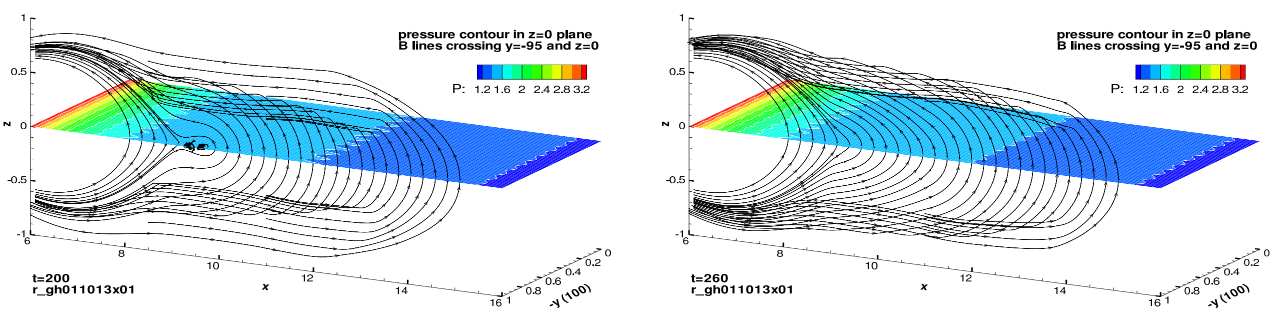

FIG. 5: Total pressure contours in the $z = 0$ plane and magnetic field lines crossing the x axis at $y = -95, z = 0$ at selected times ($t = 200, 260$).

[11] J. Birn, R. Sommer, and K. Schindler, *Astrophys. Space Sci.* **35**, 389 (1975).

[12] J. Birn, *J. Geophys. Res.* **85**, 1214 (1980).

[13] L. Janicke, *Phys. Fluids* **23**, 1843 (1980).

[14] M. Hesse and J. Birn, *J. Geophys. Res.* **99**, 8565 (1994).

[15] B. G. Harrold, A. Bhattacharjee, and X. G. Wang, *Phys. Plasmas* **2**, 3857 (1995).

[16] A. K. Sundaram and D. H. Fairfield, *J. Geophys. Res.* **102**, 19913 (1997).

[17] M. I. Sitnov, A. S. Sharma, P. N. Guzdar, et al., *J. Geophys. Res.* **107**, 1256 (2002).

[18] J. Raeder, P. Zhu, Y. Ge, et al., *J. Geophys. Res.* **115**, A00I16 (2010).

[19] P. Zhu, J. Raeder, C. C. Hegna, et al., *J. Geophys. Res. Space Physics* **118**, 653 (2013).

[20] J. W. Connor, R. J. Hastie, and J. B. Taylor, *Phys. Rev.*

Lett. **40**, 396 (1978).
[21] R. L. Dewar and A. H. Glasser, *Phys. Fluids* **26**, 3038 (1983).
[22] E. Hameiri, P. Laurence, and M. Mond, *J. Geophys. Res.* **96**, 1513 (1991).
[23] K. Schindler, in *Earth's Magnetospheric Processes*, edited by B. M. McCormac (D. Reidel, Norwell, Mass., 1972), p. 200.
[24] P. Zhu, J. Raeder, K. Germaschewski, et al., *Ann. Geophys.* **27**, 1129 (2009).
[25] C. Sovinec, A. Glasser, D. Barnes, et al., *J. Comput.Phys.* **195**, 355 (2004).
[26] P. L. Pritchett and F. V. Coroniti, *Geophys. Res. Lett.* **38**, L10102 (2011).
[27] N. Bessho and A. Bhattacharjee, in *American Geophysical Union Fall Meeting, San Francisco, CA, USA, December 3-7, 2012* (2012), abstract SM52A-04.
[28] M. I. Sitnov, N. Buzulukova, M. Swisdak, et al., *Geophys. Res. Lett.* **40**, 1 (2013).